Electronic Supplementary Material (ESI) for Energy & Environmental Science.
This journal is © The Royal Society of Chemistry 2021

Photo-assisted Charge/discharge Li-organic Battery with a Charge-separated and Redox-active C_{60}@Porous Organic Cage Cathode

Xiang Zhang,[a†] Kongzhao Su,[a†] Aya Gomaa Abdelkader Mohamed,[a,b] Caiping Liu,[a] Qingfu Sun,[a] Daqiang Yuan,[a,b,c] Yumei Wang,[d] Wenhua Xue,[d] and Yaobing Wang*[a,b,c]

[a] *CAS Key Laboratory of Design and Assembly of Functional Nanostructures, and Fujian Provincial Key Laboratory of Nanomaterials, State Key Laboratory of Structural Chemistry, Fujian Institute of Research on the Structure of Matter, Chinese Academy of Sciences, Fuzhou 350002, Fujian, P. R. China. E-mail: wangyb@fjirsm.ac.cn*

[b] *University of Chinese Academy of Sciences, Beijing 100049, P. R. China.*

[c] *Fujian Science and Technology Innovation Laboratory for Optoelectronic Information of China, Fuzhou 350108, Fujian, P. R. China.*

[d] *Beijing National Laboratory for Condensed Matter Physics Institute of Physics, Chinese Academy of Science, Beijing 100190, P. R. China.*

† These authors contributed equally to this work.

Table of Contents

1. Material Synthesis

Synthesis of POC:

POC was synthesized according to previous work.[1] C4RACHO (0.20 mmol, 162 mg) and p-phenylenediamine (0.4 mmol, 43 mg) were added into a 48 mL pressure vial containing 5 mL nitrobenzene and 15 mL chloroform, followed by heating at 65 °C with stirring for 48 hours. Afterward, methanol vapor was slowly diffused into the above mixture, giving red block single crystals at yield of ~78 % for POC. ^{1}H NMR (400 MHz, $CDCl_3$, 298 K): δ 1.04 (d, 144H), 1.60 (m, 24H), 2.10 (t, 48H), 4.65 (t, 24H), 7.37 (s, 24H), 7.40 (s, 48H), 9.18 (s, 24H), 10.38 (s, 24H), 16.21 (s, 24H). p.p.m. ESI-TOF-MS calculated for POC, $C_{360}H_{384}N_{24}O_{48}$ $[M-2H]^{2-}$ 2905.4178, found 2905.3963.

Synthesis of C_{60}@POC:

C_{60}@POC was synthesized as follows: C_{60} (0.05 mmol, 36 mg) was firstly dissolved in toluene (10 mL) and chloroform (10 mL) in a 38 mL pressure vial, followed by adding C4RACHO (0.10 mmol, 82 mg) and p-phenylenediamine (0.20 mmol, 21.5 mg). The mixture was sealed and heated to 70 °C with stirring for 48 h. Afterward, methanol vapor was slowly diffused into the above-mentioned mixture, affording dark red precipitate. The precipitate was further dissolved in tetrahydrofuran to filter off the unencapsulated C_{60}. After vacuum drying, about 0.76 g of dark red product for C_{60}@POC was obtained.

2. Characterization:

The morphology and elementary analysis of the samples were obtained by field-emission scanning electron microscopy (JSM 6700F) equipped with an energydispersive spectroscopy analyzer. Elemental mapping images were recorded on FEI talos F200i microscope from Bruker. Cryo-TEM was conducted on Titan Krios G3i 300kV Cryo-EM. ^{1}H and ^{13}C NMR spectra were obtained on a Burker AVANCE 400 (400 MHz) spectrometer. High-resolution electrospray ionization time of flight mass spectrometry (ESI-TOF-MS) spectra were recorded on a MaXis™ 4G instrument from Bruker. N_2 adsorption-desorption measurements were carried out by using automatic volumetric adsorption equipment (Micromeritics, ASAP2020). UV-Vis-NIR spectra were performed on PerkinElmer Lambda-950 UV-Vis spectrometer using $BaSO_4$ as reference. Fluorescence emission spectrum were recorded on FLS920 spectrometer (Edinburgh Instruments, UK). Ultraviolet Photoelectron Spectroscopy (UPS) was performed by ESCALAB 250Xi (ThermoFisher, USA). Electron paramagnetic resonance (EPR) spectra were obtained from Bruker ELEXSYS E500 spectrometer with incident light.

3. Femtosecond transient absorption spectroscopy

Fs-TA measurements were performed based on a femtosecond regenerative amplified Ti: sapphire laser system from Coherent (800 nm, 100 fs, 6 Mj per pulse, and 1 kHz repetition rate). The 800 nm output pulse from the regenerative amplifier was split into two parts with a beam splitter. The reflected part was used to pump a TOPAS Optical Parametric Amplifier (OPA), which generates a wavelength-tunable laser pulse from 250 nm to 2.5 mm as the pump beam. The transmitted 800 nm beam was attenuated with a neutral density filter and focused into a rotating CaF_2 disk to generate a white light continuum (WLC) from 350 nm to 800 nm

used for the probe beam. The probe beam was focused with an Al parabolic reflector onto the sample. After the sample, the probe beam was collimated and then focused into a fiber-coupled spectrometer and detected at a frequency of 1 kHz. The intensity of the pump pulse used in the experiment was controlled by a variable neutral-density filter wheel. The delay between the pump and probe pulses was controlled by a motorized delay stage. The pump pulses were chopped by a synchronized chopper at 500 Hz.

4. The HOMO and LUMO energy levels evaluation

The HOMO and LUMO energy levels of the materials were evaluated by cyclic voltammograms (CV) measurements. CV was conducted in a three-electrode configuration with a glass carbon electrode (diameter: 4 mm) as the working electrode, a Pt plate as counter electrode, and a silver wire pseudo-reference electrode. The electrolyte was acetonitrile containing with 0.10 M Tetrabutylammonium hexafluorophosphate (TBAPF6). The potential range was between −2.3 V and +1.3 V (vs. Fc/Fc^{+}) at a scan rate of 50 mV s^{-1}. The HOMO and LUMO levels of the materials can be determined by the onset potentials of the oxidation/ reduction potentials.

5. Electrode preparation and battery fabrication

Electrochemical performance of POC and C_{60}@POC was investigated in CR2025 coin cells, which comprises a POC or C_{60}@POC cathode, a Li foil anode and a polypropylene seperator (Celgard2400). Cathodes were prepared by making a slurry containing active material, carbon nanotube and poly(vinylidene difluoride) (PVDF) in the ratio of 5 : 4 : 1 in 1-methyl-2-pyrrolidinone (NMP). The slurry was then cast onto stainless steel (SUS 304) foil, followed by drying at 60 °C in a vacuum oven for 24 h. The mass loading of the active material

in each electrode was ~1.5 mg cm^{-2}. The electrolyte was 1 M LiTFSI dissolved in a mixture of 1,3-dioxolane (DOL) and 1,2-dimethoxyethane (DME) (1:1 in volume).

Photoelectrochemical performances of POC and C_{60}@POC were investigated in coin cells with nine holes at the cathode shells, which enables the illumination on the cathode. Also, a home-made lithium-ion battery was assembled, where the cathode was a piece of FTO coated by POC, C_{60}@POC and a mixture of of C4RACHO, phenylenediamine, and fullerene with 2 : 4 : 1 molar ratio, and the anode was Li foil supported by copper foil as current collector. The cathode and anode were soaked by the same electrolyte as that in the coin cell, and separated by a polypropylene membrane. Afterward, the above components were bonded together by a clamp, followed by sealing into a glass bottle to ensure insulation from oxygen and water.

6. Electrochemical and photoelectrochemical measurements

Electrochemical impedance spectroscopy (EIS) measurememts were performed over the frequency range of 0.1 Hz~1 MHz with an input voltage amplitude of 5 mV. A 300 W Xe lamp (PLSSXE300, Perfectlight, China) equipped with an AM 1.5G filter was used as the light source, and the introduced light power is ~200 mW cm^{-2}. EIS was recorded on CHI660e electrochemical working station (CH Instrument Inc.), and galvanostatic measurements were conducted on a battery test system (LAND-V34, Land Electronic Co, Ltd, Wuhan). *I-V* curves were obtained by recording voltages at different discharge/charge current (0.01, 0.05, 0.1, 0.2, 0.5, 1.0, 1.5, 2.0 and 3.0 mA cm^{-2}), and each discharge/charge current was maintained for 5s. *I-P* curves was obtained by multiplying currents and the corresponding voltages.

7. Computational calculation

To explore the effect of fullerene on cage, the molecular orbital properties of POC and C_{60}@POC with two entrapped C_{60} were investigated by the density functional theory (DFT) calculations. At first, their geometries were fully optimized by using the Dmol3 module program,[2] in which the generalized gradient approximation (GGA), with the Perdew, Burke, and Ernzerhof (PBE) functional,[3] double numerical plus d-functions (DND) basis set, the Grimme method for DFT-D dispersion corrections[4] and a high convergence criterion were adopted. And then, the frontier molecular orbitals of POC and C_{60}@POC with two entrapped C_{60} were calculated using the B3LYP functional and 6-31G(d) basis sets implemented in the Gaussian 16 program.[5,6]

8. Supplementary Figures

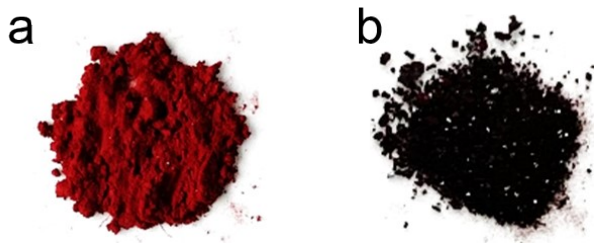

Fig. S1 Digital photos of (a) POC and (b) C_{60}@POC powder.

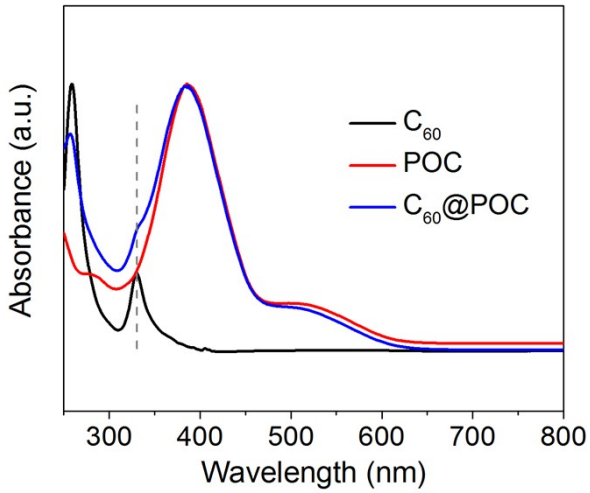

Fig. S2 Liquid phase UV-Vis spectra of C_{60}, POC and C_{60}@POC in $CHCl_3$.

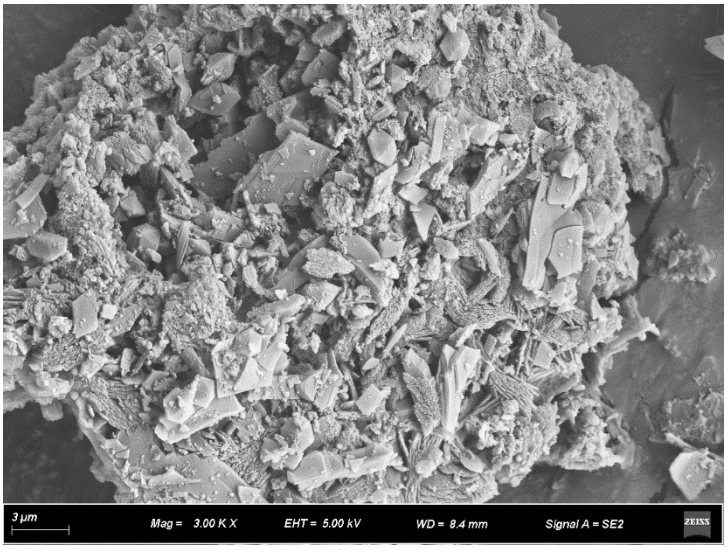

Fig. S3 SEM image of C_{60}@POC.

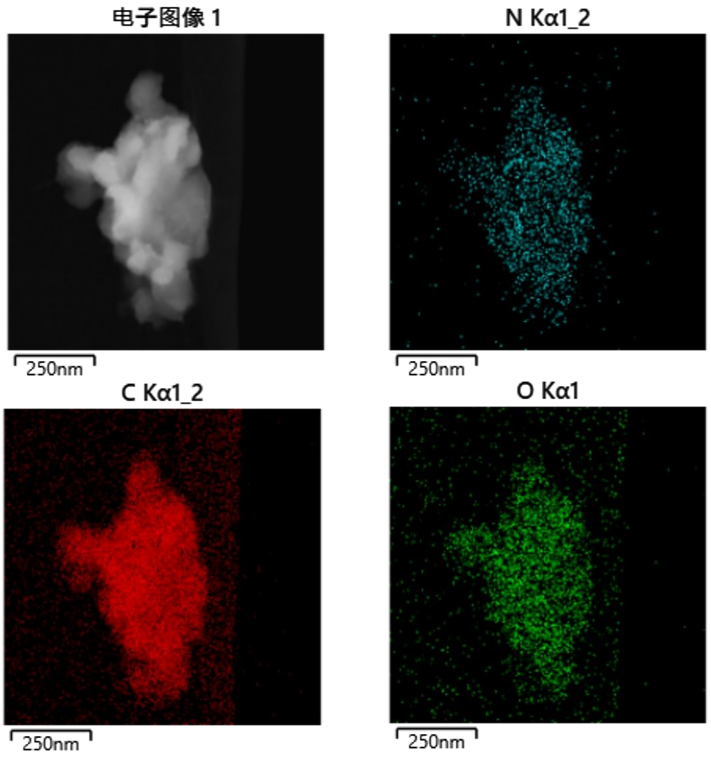

Fig. S4 Elemental mapping images of C_{60}@POC.

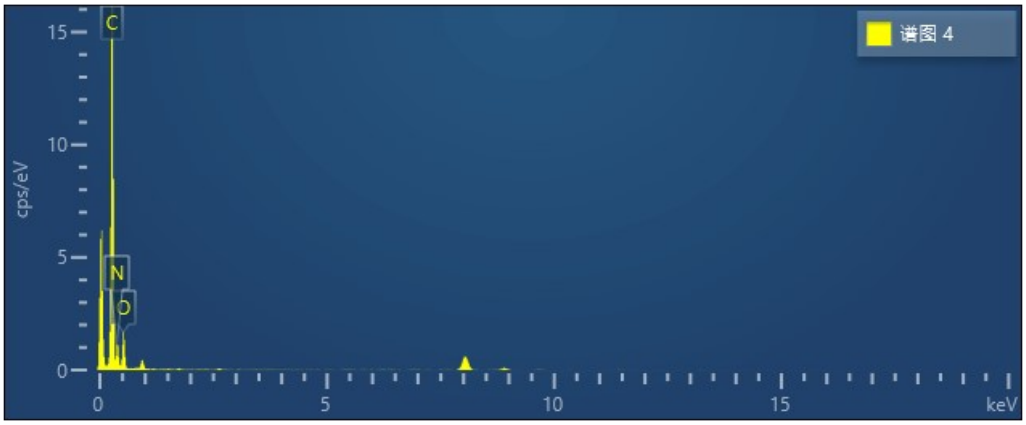

Elements	Wt.%	At.%
C	92.56	94.02
N	2.82	2.46
O	4.61	3.52
Total:	100.00	100.00

Fig. S5 EDS results of C_{60}@POC.

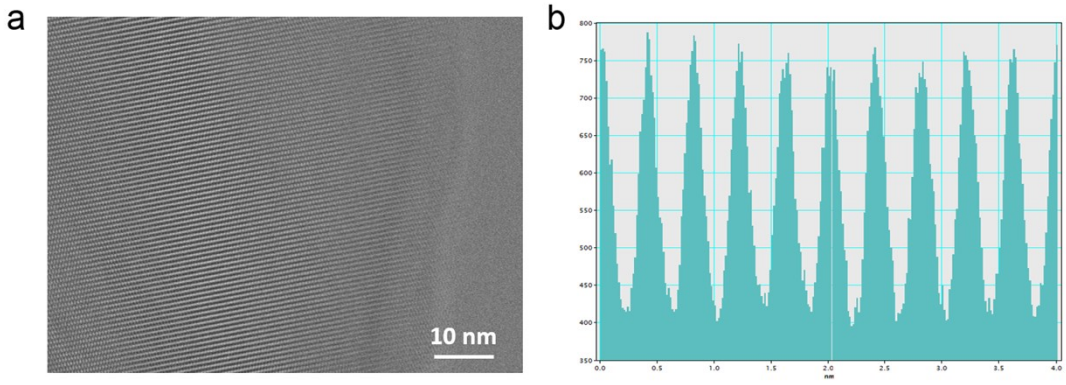

Fig. S6 (a) Cryo-TEM image of C_{60}@POC. (b) The corresponding interplanar spacing.

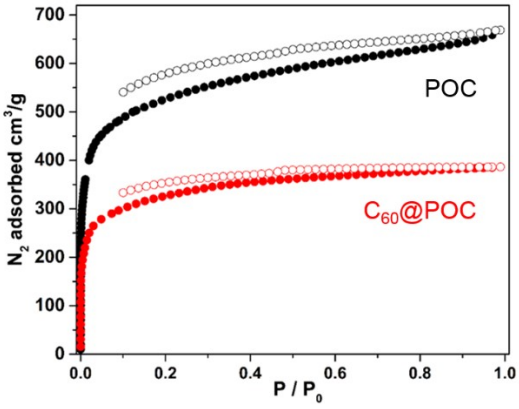

Fig. S7 N_2 absorption-desorption curves of POC and C_{60}@POC.

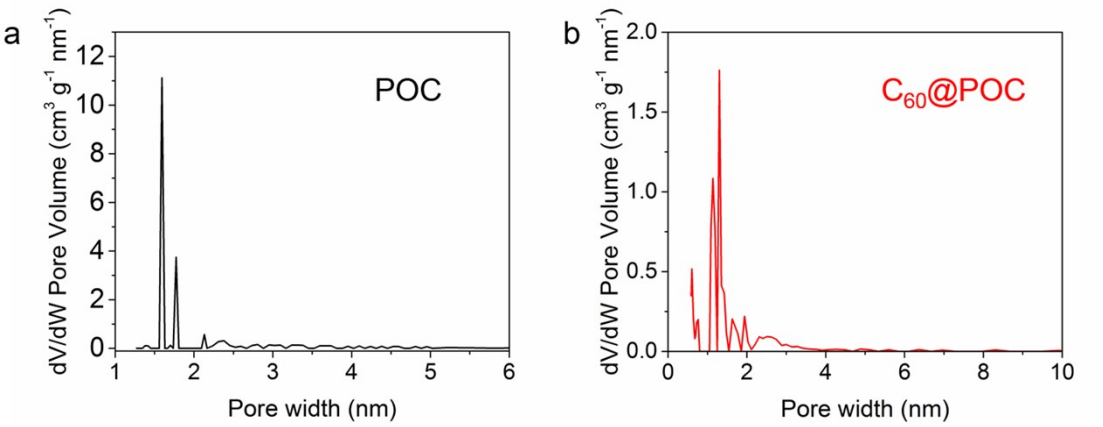

Fig. S8 Pore size and pore volume of POC and C_{60}@POC.

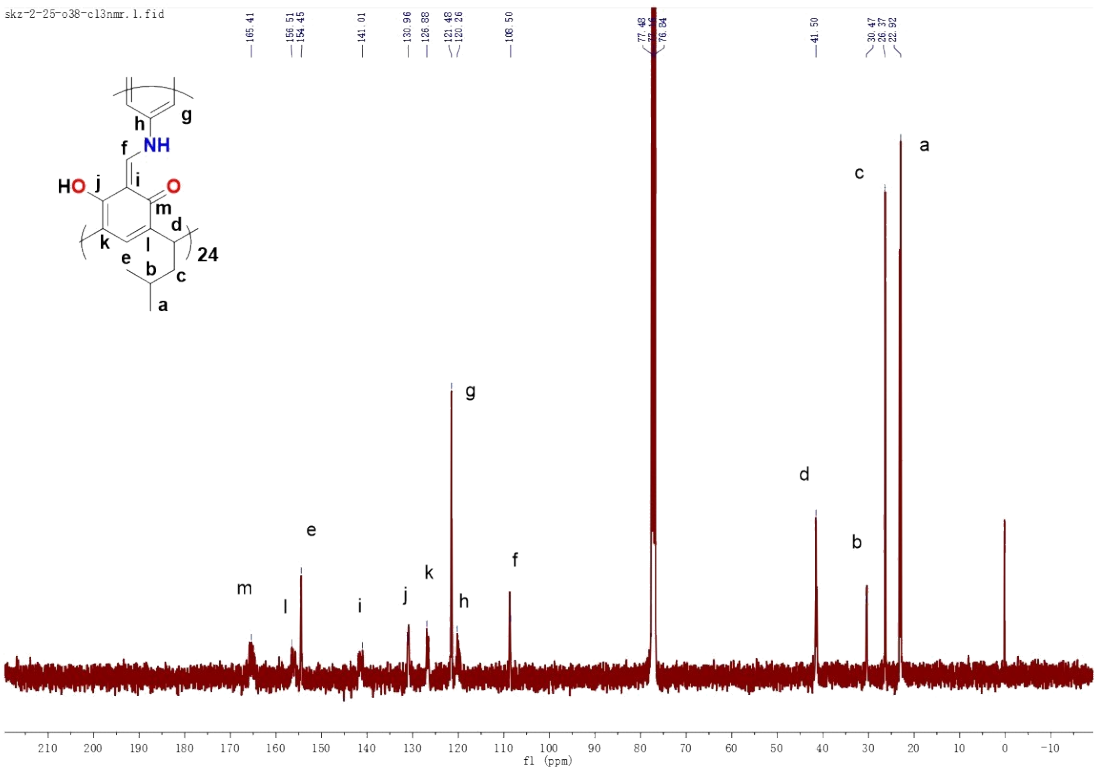

Fig. S9 ^{13}C NMR of POC ($CDCl_3$, 400 MHz, 298 K).

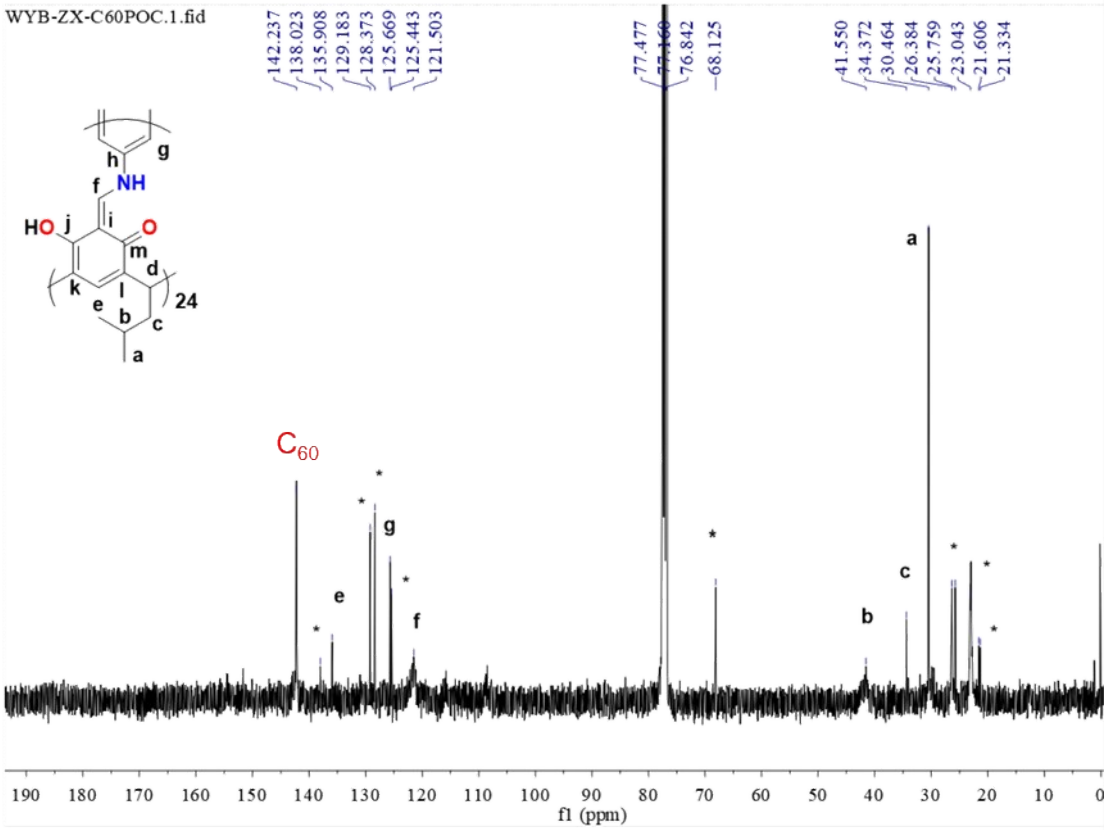

Fig. S10 ^{13}C NMR of C_{60}@POC ($CDCl_3$, 400 MHz, 298 K). *Indicates residual solvent chloroform and tetrahydrofuran.

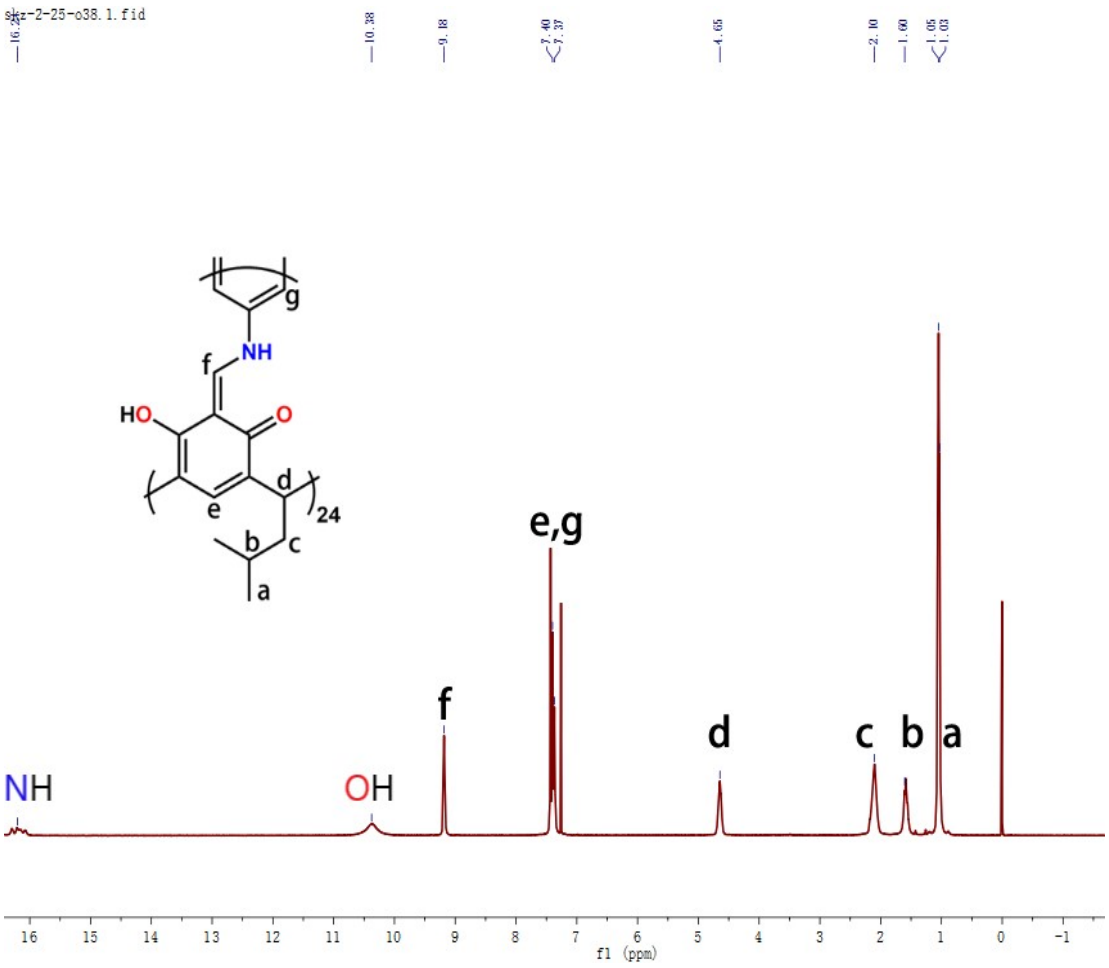

Fig. S11 ^{1}H NMR of POC ($CDCl_3$, 400 MHz, 298 K).

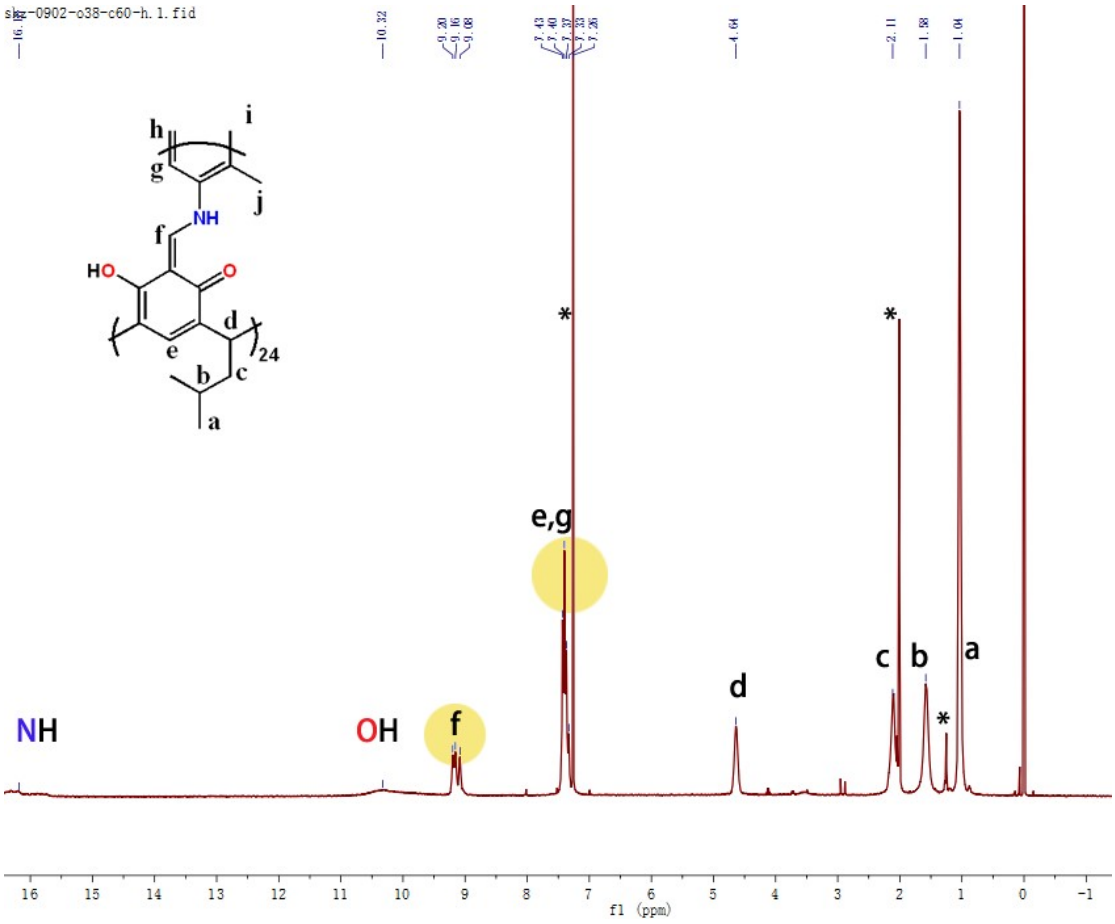

Fig. S12 ^{1}H NMR of C_{60}@POC ($CDCl_3$, 400 MHz, 298 K). Yellow regions indicate changes in chemical shift upon C_{60} encapsulation. *Indicates residual solvent chloroform and tetrahydrofuran.

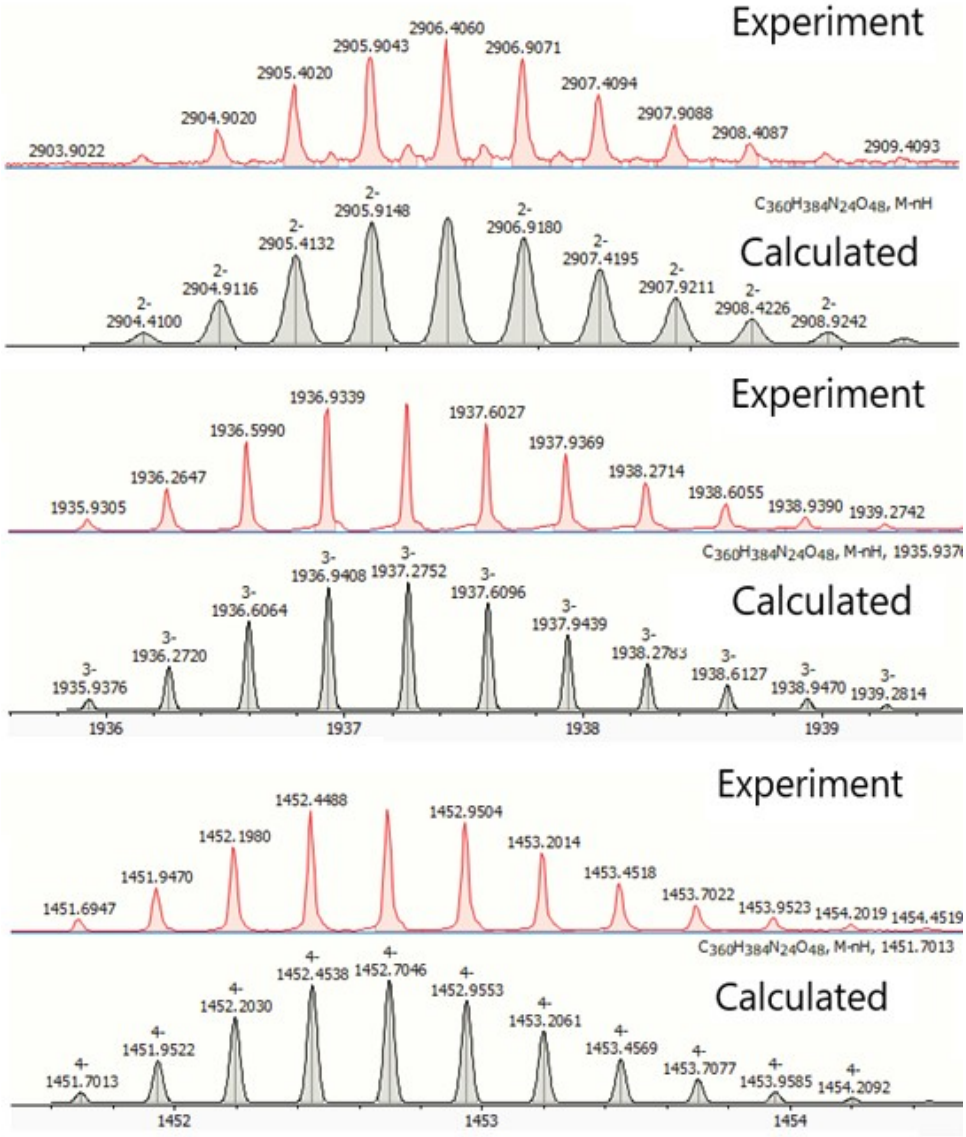

Fig. S13 ESI-TOF-MS spectrum of POC recorded in $CHCl_3$.

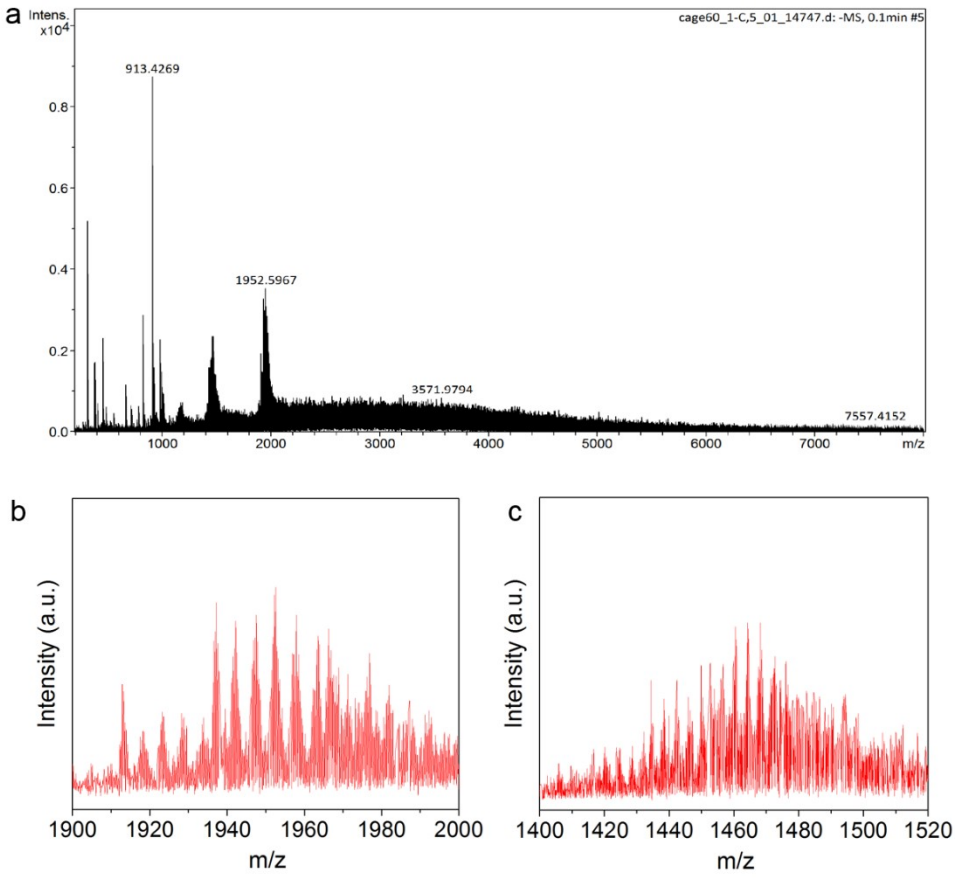

Fig. S14 ESI-TOF-MS spectra of C_{60}@POC recorded in $CHCl_3$. a) Full spectrum. b) From 1900 to 2000, m/z. c) From 1400 to 1520, m/z.

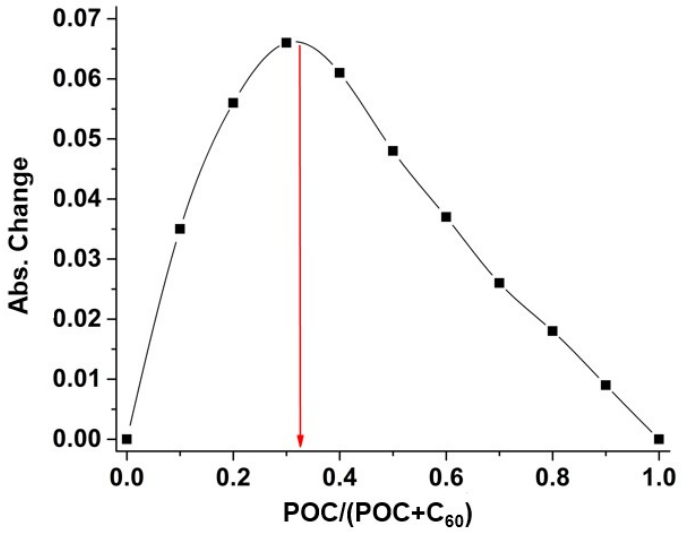

Fig. S15 Job's plot at 331 nm for the host-guest formation of POC with C_{60}.

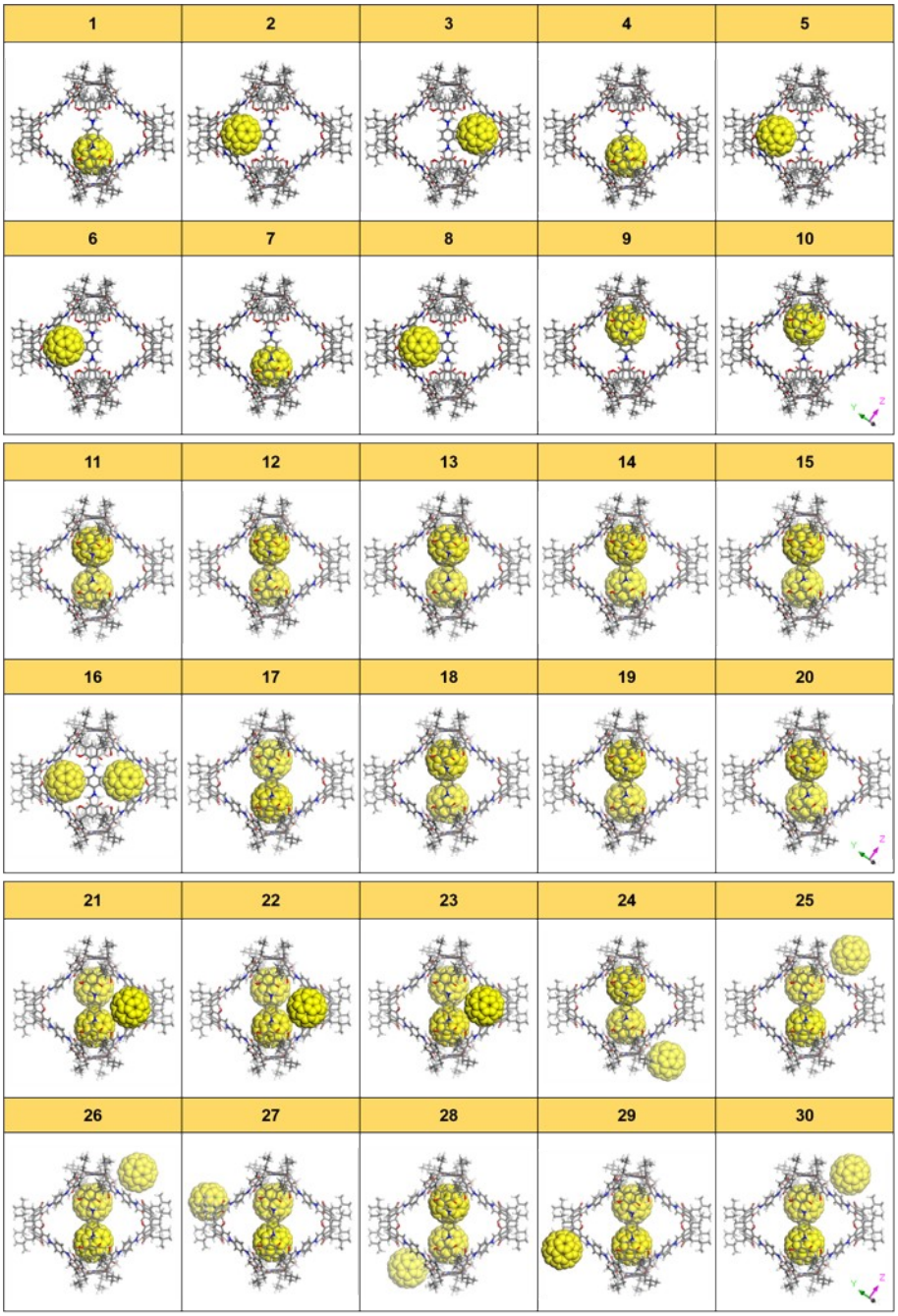

Fig. S16 Structures of C_{60}@POC with one, two or three C_{60} molecules.

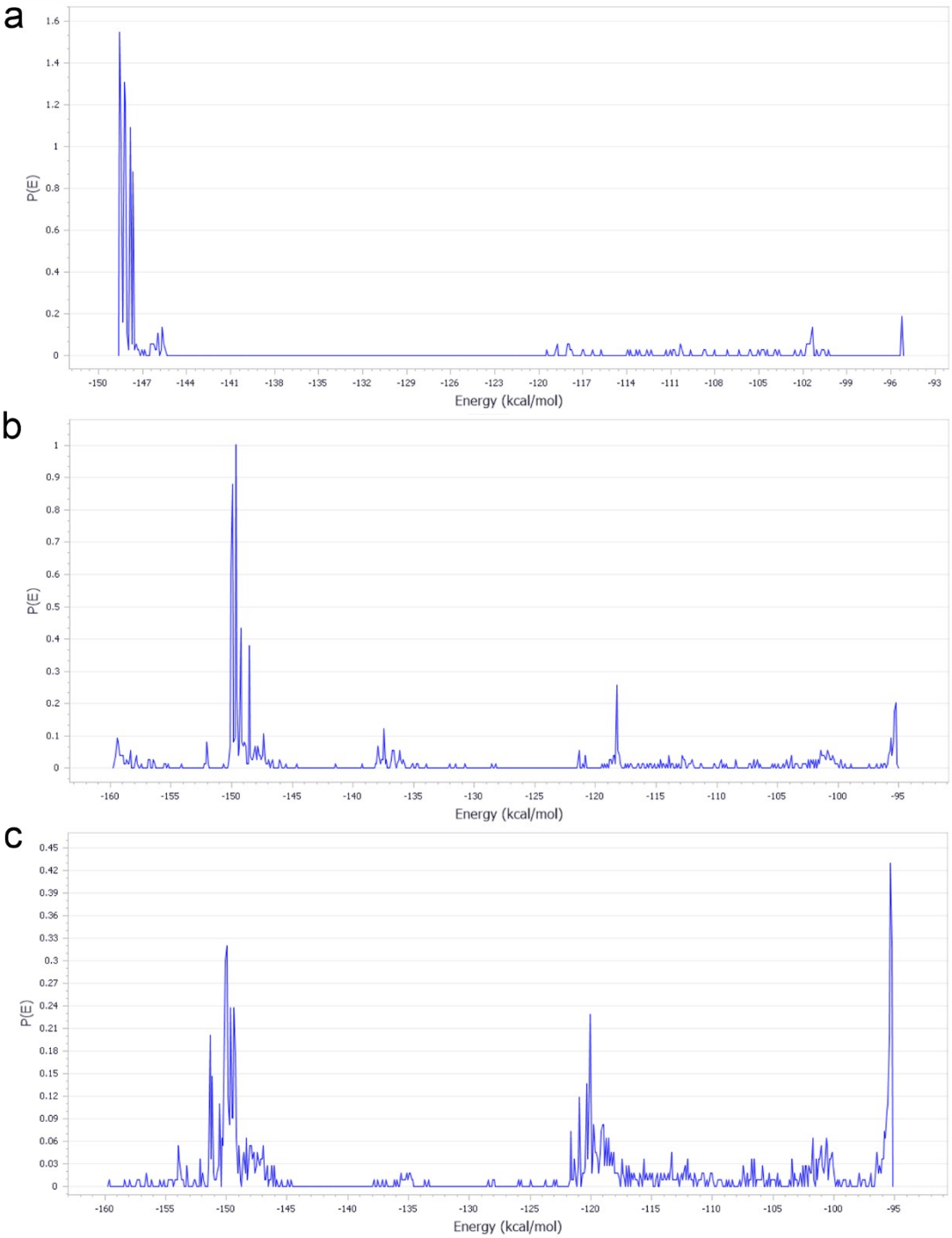

Fig. S17 Energy distribution of C_{60}@POC with (a) one C_{60}, (b) two C_{60}, and (c) three C_{60} molecules.

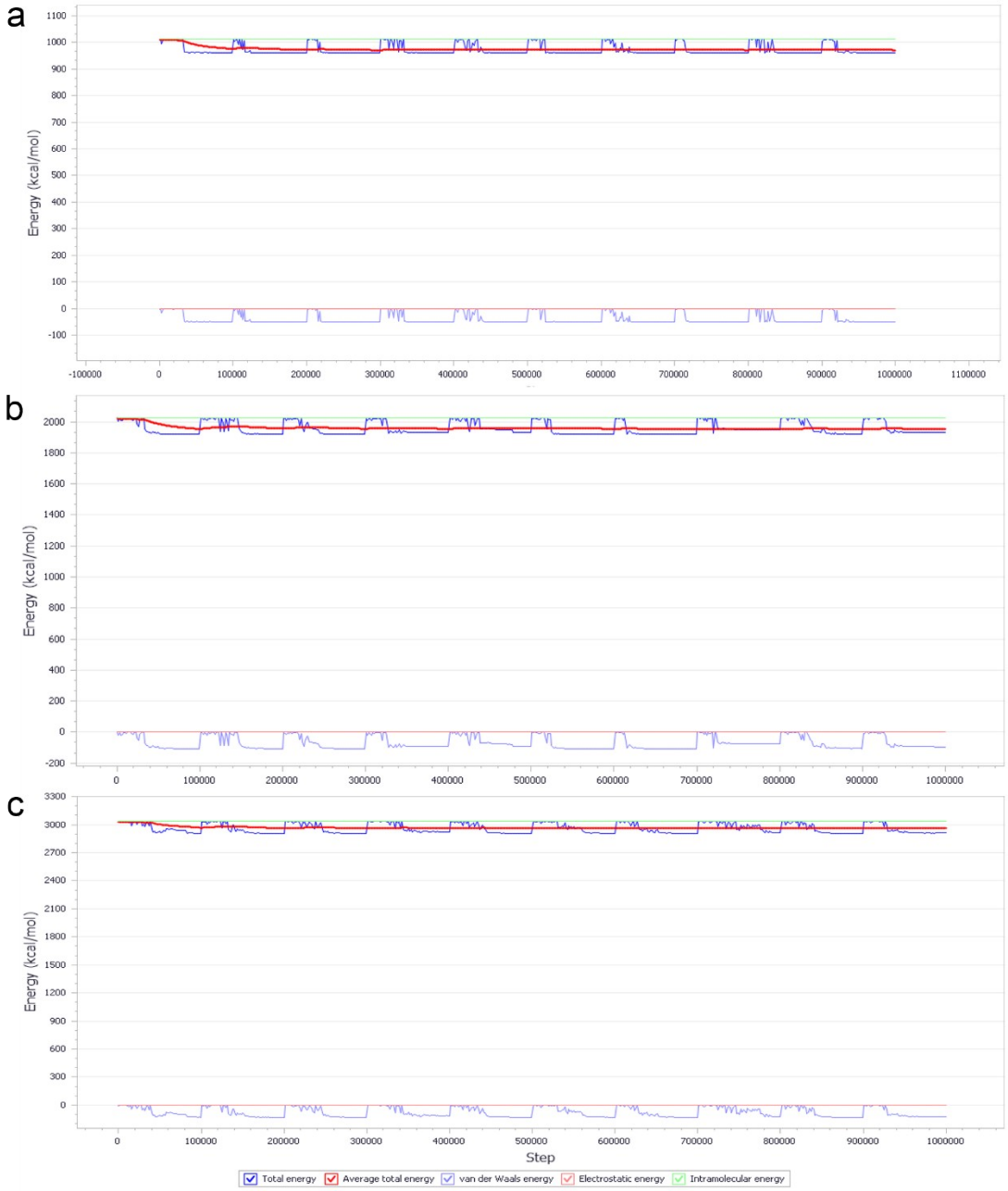

Fig. S18 Total energy of C_{60}@POC with (a) one C_{60}, (b) two C_{60}, and (c) three C_{60} molecules.

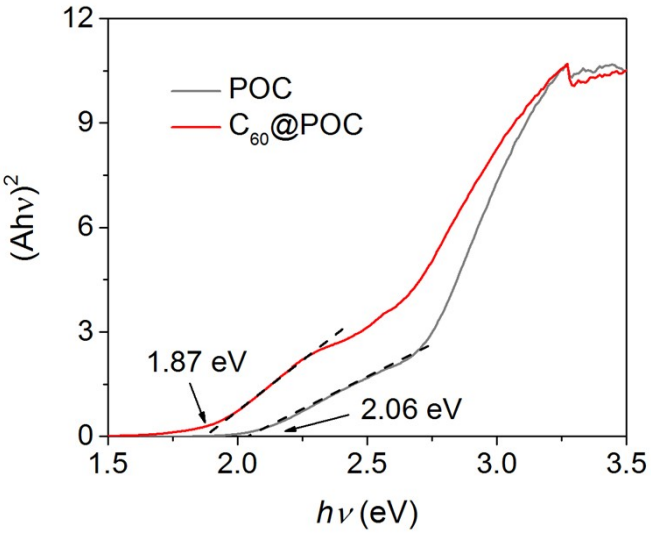

Fig. S19 Tauc-plots of POC and C_{60}@POC.

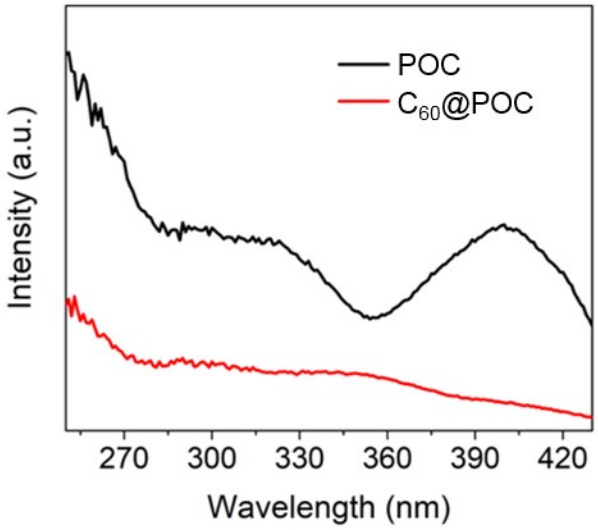

Fig. S20 FL excitation spectra of C_{60}@POC and POC.

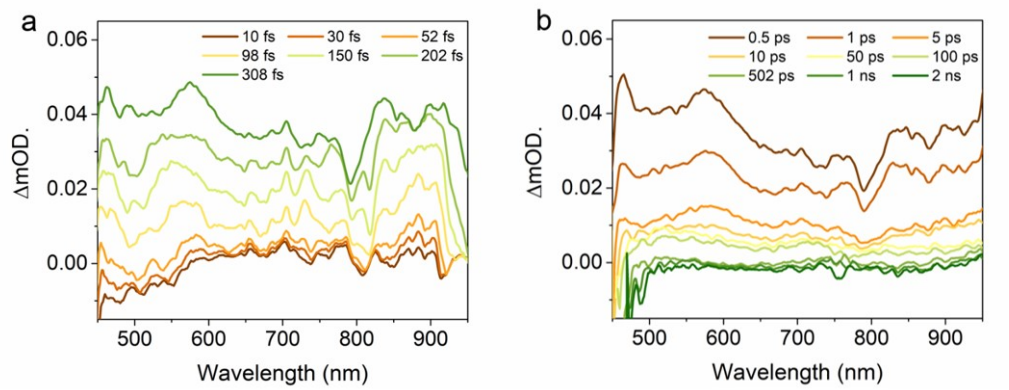

Fig. S22 fs-TA spectra of POC.

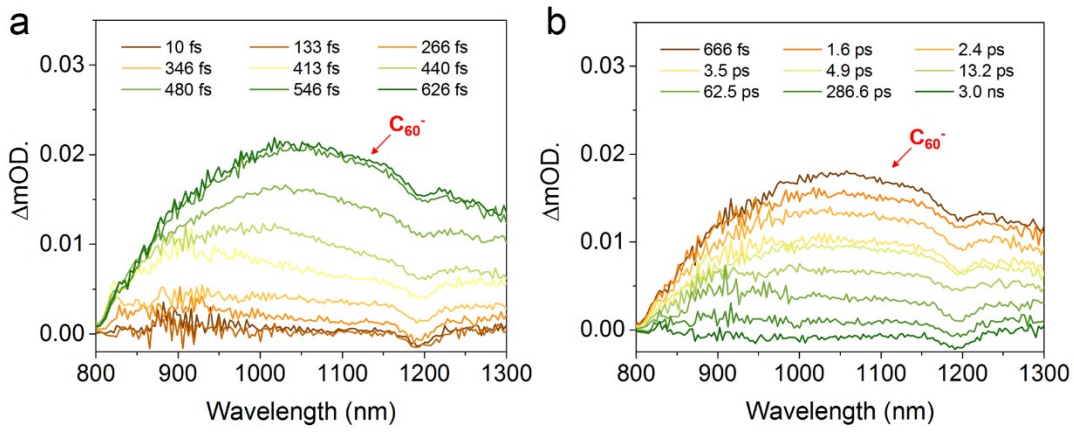

Fig. S22 fs-TA spectroscopy of the C_{60}@POC in the NIR region. (a) From 10 fs to 626 fs. (b) From 666 fs to 3.0 ns. The peaks at around 1100 nm indicate the presence of C_{60}^{-} radical anion.

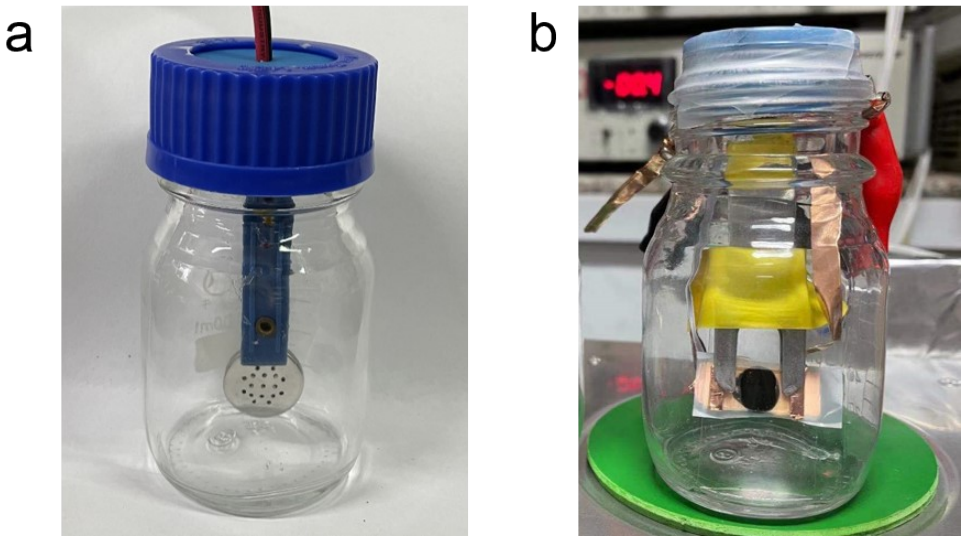

Fig. S23 (a) Device for photo-assisted lithium-ion battery. (b) Home-made lithium-ion battery.

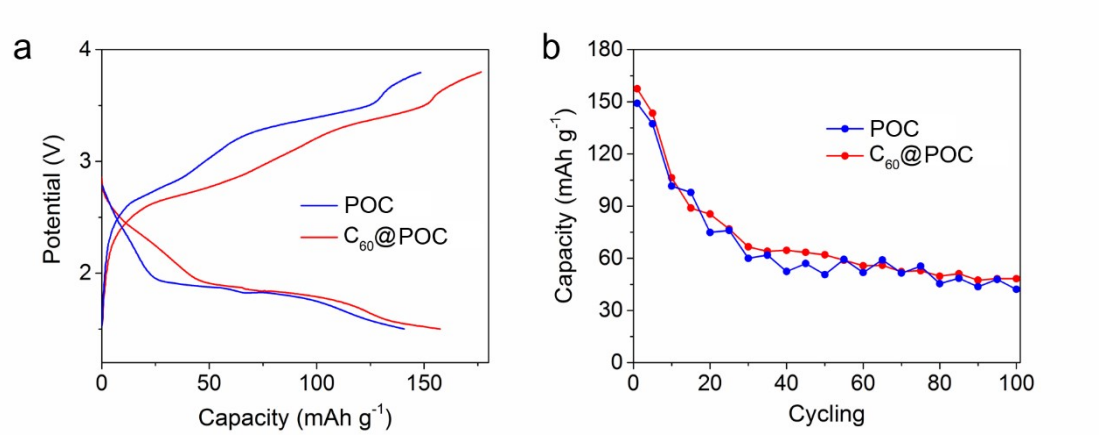

Fig. S24 Discharge/charge curves (a) and cyclic discharge capacities (b) of POC and C_{60}@POC.

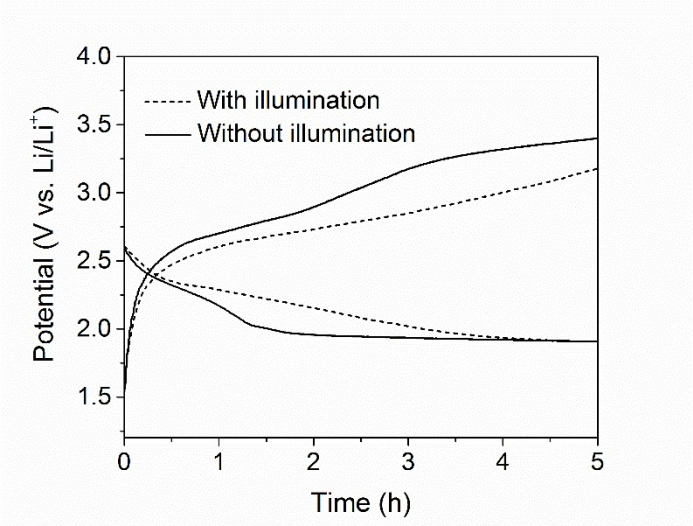

Fig. S25 Charge and discharge curves of POC with or without illumination. No obvious contribution of light in discharge process can be observed, while the charge platform is dropped by 0.3 V (3.34 – 3.04 V) under light, therefore demonstrating a 5.6% increase of round-trip efficiency.

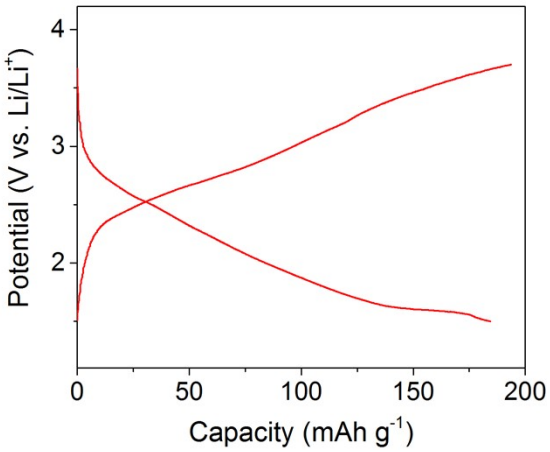

Fig. S26 Charge and discharge curves of C_{60}@POC under illumination. The photo-assisted discharge/charge capacity is 184/193 mAh g^{-1}, which is 115%/114% of the discharge/charge capacity without illumination.

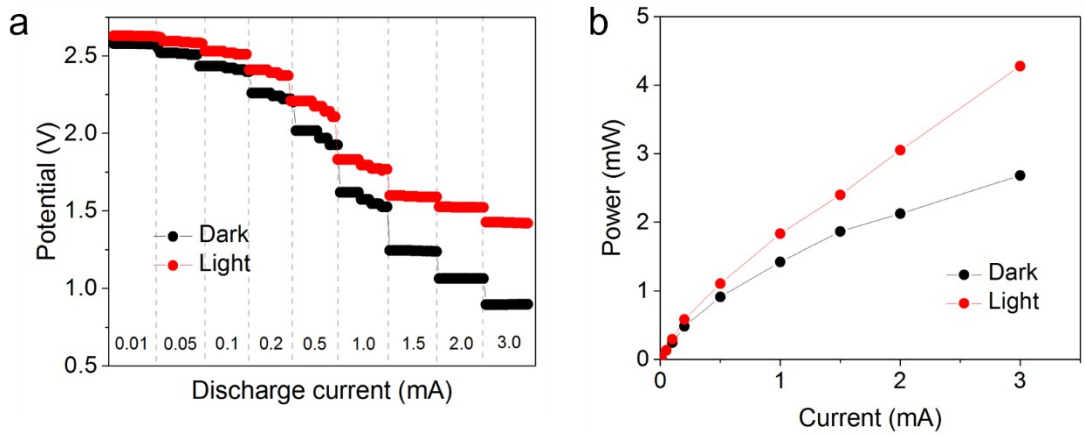

Fig. S27 (a) *I-V* curve of POC during discharge. (b) *I-P* curve of POC during discharge. In light, the discharge voltage of POC maintains 1.42 V at 3 mA cm^{-2} with a 0.52 V of voltage lifting compared to 0.90 V in dark condition. The corresponding output powers of POC in dark/light condition at 3 mA cm^{-2} are 2.68 and 4.27 mW cm^{-2} (Figure 3d), demonstrating a 59.3% increase in output power under illumination.

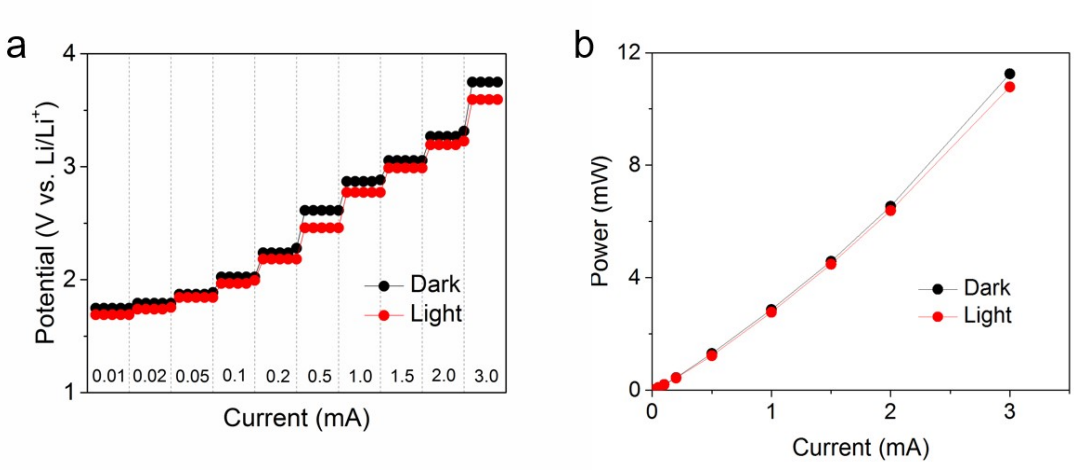

Fig. S28 (a) *I-V* curve of POC during charge. (b) *I-P* curve of POC during charge. In light, the charge voltage of POC is 3.59 V at 3 mA cm^{-2} with a 0.16 V of voltage decrease compared to 3.75 V in dark condition. The corresponding input powers of POC in dark/light condition at 3 mA cm^{-2} are 11.25 and 10.78 mW cm^{-2} (Figure 3f), demonstrating a 4.2% decrease in input power under illumination.

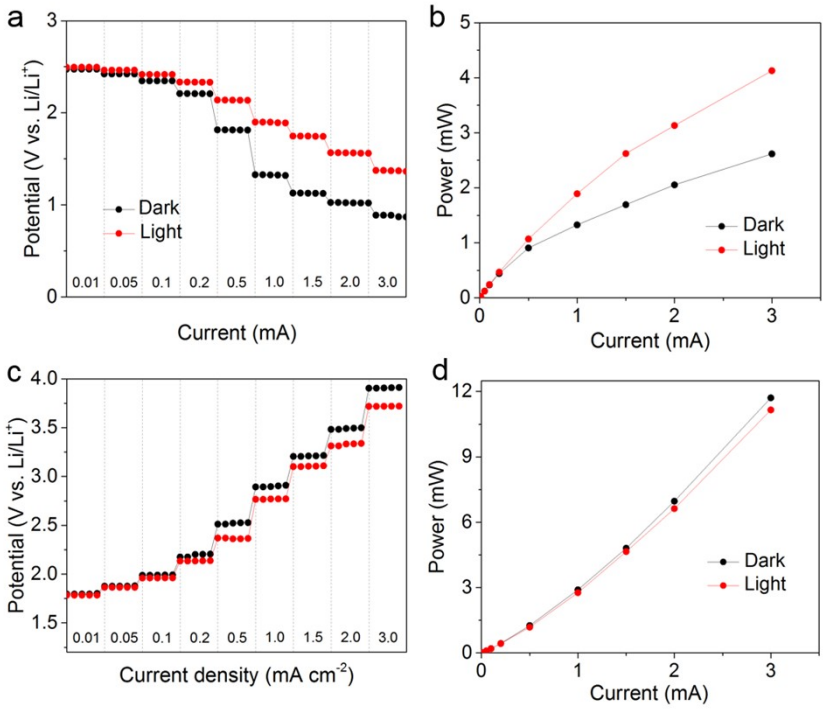

Fig. S29 Solar conversion and storage performances of the battery using a mixture of C4RACHO, phenylenediamine, and C_{60} as the cathode. (a, b) *I-V* and *I-P* curves during discharge. (c, d) *I-V* and *I-P* curves during charge.

9. Supplementary Tables

Table S1. Comparison of experimental and calculated mass data of C_{60}@POC.

Fragment	Calculated	Experimental
$[C_{360}H_{384}N_{24}O_{48}+2C_{60}\ 3(CHCl_3)1(H_2O)-H]^{4-}$	1904.63	1903.89
$[C_{360}H_{384}N_{24}O_{48}+2C_{60}\ 3(CHCl_3)3(H_2O)-H]^{4-}$	1913.64	1913.57
$[C_{360}H_{384}N_{24}O_{48}+2C_{60}\ 3(CHCl_3)4(H_2O)-H]^{4-}$	1918.14	1918.24
$[C_{360}H_{384}N_{24}O_{48}+2C_{60}\ 3(CHCl_3)5(H_2O)-H]^{4-}$	1922.65	1922.56
$[C_{360}H_{384}N_{24}O_{48}+2C_{60}\ 3(CHCl_3)6(H_2O)-H]^{4-}$	1927.15	1927.56
$[C_{360}H_{384}N_{24}O_{48}+2C_{60}\ 4(CHCl_3)-H]^{4-}$	1932.45	1932.45
$[C_{360}H_{384}N_{24}O_{48}+2C_{60}\ 4(CHCl_3)1(H_2O)-H]^{4-}$	1936.95	1936.92
$[C_{360}H_{384}N_{24}O_{48}+2C_{60}\ 4(CHCl_3)2(H_2O)-H]^{4-}$	1941.46	1942.25
$[C_{360}H_{384}N_{24}O_{48}+2C_{60}\ 4(CHCl_3)4(H_2O)-H]^{4-}$	1947.62	1947.25
$[C_{360}H_{384}N_{24}O_{48}+2C_{60}\ 4(CHCl_3)5(H_2O)-H]^{4-}$	1952.12	1952.58
$[C_{360}H_{384}N_{24}O_{48}+2C_{60}\ 4(CHCl_3)6(H_2O)-H]^{4-}$	1956.63	1956.90
$[C_{360}H_{384}N_{24}O_{48}+2C_{60}\ 5(CHCl_3)-H]^{4-}$	1962.29	1962.91
$[C_{360}H_{384}N_{24}O_{48}+2C_{60}\ 5(CHCl_3)1(H_2O)-H]^{4-}$	1966.80	1966.27
$[C_{360}H_{384}N_{24}O_{48}+2C_{60}\ 5(CHCl_3)2(H_2O)-H]^{4-}$	1971.30	1971.26
$[C_{360}H_{384}N_{24}O_{48}+2C_{60}\ 5(CHCl_3)4(H_2O)-H]^{4-}$	1980.30	1981.26
$[C_{360}H_{384}N_{24}O_{48}+2C_{60}\ 5(CHCl_3)6(H_2O)-H]^{4-}$	1989.32	1988.48

Fragment	Calculated	Experimental
$[C_{360}H_{384}N_{24}O_{48}+2C_{60}-H]^{5-}$	1450.26	1450.42
$[C_{360}H_{384}N_{24}O_{48}+2C_{60}\ 4(H_2O)-H]^{5-}$	1464.67	1464.19
$[C_{360}H_{384}N_{24}O_{48}+2C_{60}\ 1(CHCl_3)-H]^{5-}$	1474.13	1473.92
$[C_{360}H_{384}N_{24}O_{48}+2C_{60}\ 1(CHCl_3)1(H_2O)-H]^{5-}$	1477.73	1476.43
$[C_{360}H_{384}N_{24}O_{48}+2C_{60}\ 1(CHCl_3)2(H_2O)-H]^{5-}$	1481.34	1480.18
$[C_{360}H_{384}N_{24}O_{48}+2C_{60}\ 1(CHCl_3)3(H_2O)-H]^{5-}$	1484.94	1484.94
$[C_{360}H_{384}N_{24}O_{48}+2C_{60}\ 1(CHCl_3)4(H_2O)-H]^{5-}$	1488.54	1488.68
$[C_{360}H_{384}N_{24}O_{48}+2C_{60}\ 2(CHCl_3)-H]^{5-}$	1498.01	1497.94
$[C_{360}H_{384}N_{24}O_{48}+2C_{60}\ 2(CHCl_3)1(H_2O)-H]^{5-}$	1501.61	1500.70
$[C_{360}H_{384}N_{24}O_{48}+2C_{60}\ 2(CHCl_3)2(H_2O)-H]^{5-}$	1505.21	1504.68
$[C_{360}H_{384}N_{24}O_{48}+2C_{60}\ 2(CHCl_3)4(H_2O)-H]^{5-}$	1512.42	1511.69
$[C_{360}H_{384}N_{24}O_{48}+2C_{60}\ 3(CHCl_3)-H]^{5-}$	1521.88	1521.21
$[C_{360}H_{384}N_{24}O_{48}+2C_{60}\ 3(CHCl_3)2(H_2O)-H]^{5-}$	1529.09	1530.97

Table S2. Structure energy of C_{60}@POC.

Structure	Total energy	Asorption energy	Rigid asorption energy	Deformation energy	C_{60}:dEad/dNi
1	863.947	-148.588	-53.3834	-95.2042	-148.588
2	864.148	-148.387	-53.1781	-95.2085	-148.387
3	864.379	-148.156	-52.9666	-95.1898	-148.156
4	864.709	-147.826	-52.6334	-95.1926	-147.826
5	864.917	-147.618	-52.4319	-95.1859	-147.618
6	865.281	-147.254	-52.0718	-95.1824	-147.254
7	865.492	-147.043	-51.864	-95.1795	-147.043
8	865.712	-146.823	-51.6583	-95.1645	-146.823
9	866.041	-146.494	-51.3034	-95.191	-146.494
10	866.393	-146.142	-50.9392	-95.2027	-146.142
11	1726.466	-298.605	-108.174	-190.431	-150.05
12	1726.882	-298.189	-107.782	-190.406	-149.635
13	1727.082	-297.989	-107.555	-190.434	-149.491
14	1727.316	-297.755	-107.344	-190.411	-149.234
15	1727.551	-297.52	-107.121	-190.399	-148.991
16	1727.788	-297.283	-106.887	-190.396	-148.832
17	1728.083	-296.988	-106.588	-190.4	-148.822
18	1728.316	-296.755	-106.391	-190.364	-148.973
19	1728.543	-296.528	-106.139	-190.388	-148.867
20	1728.907	-296.164	-105.782	-190.382	-148.901
21	2617.975	-419.655	-133.987	-285.668	-121.679
22	2618.263	-419.367	-133.729	-285.637	-121.392
23	2618.665	-418.965	-133.317	-285.647	-121.227
24	2618.883	-418.747	-133.058	-285.689	-121.002
25	2619.102	-418.528	-132.826	-285.703	-120.331
26	2619.405	-418.225	-132.532	-285.693	-120.25
27	2619.715	-417.915	-132.224	-285.691	-119.84
28	2619.917	-417.712	-132.061	-285.652	-119.902
29	2620.138	-417.492	-131.799	-285.693	-119.159
30	2620.436	-417.193	-131.525	-285.669	-119.002

Table S3. Photoluminescence lifetimes of POC and C_{60}@POC.

Sample	τ_S (ps)	τ_{CS} (ps)	τ_{CR} (ps)	$\tau_{average}$ (ps)
POC	0.49	178.49	3.95	3.56
C_{60}@POC	0.71	20.83	171.17	142.60

Table S4. Comparison of the resistances of POC and C_{60}@POC in dark/light conditions.

	R_s (Ω)[a]		R_{ct} (Ω)[b]	
	Dark	Light	Dark	Light
C_{60}@POC	8.4	8.1	32.7	16.5
POC	12.3	10.7	45.2	36.9

[a] Resistance of the electrolyte.

[b] Resistance of the charge transfer.

Table S5. Photoluminescence lifetimes of the reported photoelectrode materials for photo-assisted metal-ion battery and the corresponding solar to electrochemical energy storage performances.

Photoelectrode	τ_{CS} (ps)	τ_{CR} (ps)	$\tau_{average}$ (ps)	Battery System	$\Delta V_{dis.}$[a] (V)	$\Delta V_{cha.}$[b] (V)	$\eta_{conversion}$[c] (%)	$\eta_{round\text{-}trip}$[d] (%)	Cycling stability	Refs.
N719 dye/$LiFePO_4$	-	-	-	Li	-	-	0.06-0.08	-	15	7
$(C_6H_9C_2H_4NH_3)_2PbI_4$	-	-	-	Li	~ 0.5	-	~ 0.034	-	10	8
TiO_2/dye/Cu_2S	-	-	-	Li	~ 0.1	~ 0.4	~ 0.1	~ 30.6	10	9
rGO/P3HT/V_2O_5/Ag	-	-	-	Li	~ 0.15	~ 0.15	0.2	~ 8.0	200	10
Tetrakislawsone	-	-	-	Li	0	0.05	0.7	~ 1.0	~ 500	11
NT-COF	10.8	395.0	-	Li	0.5	0.5	-	38.7	100	12
Li_xTiO_2 nanoparticle	-	-	97	Li	0.1	0.2	0.5	-	7	13
FTO/rGO/VO_2/Ag	-	-	-	Zn	~0.05	~0.05	0.18	~5.0	1000	14
CF/ZnO/MoS_2	-	-	-	Zn	0.15	0.06	~0.2	~5.0	200	15
C_{60}@POC POC	20.8 178.5	171.2 4.0	142.6 3.6	Li	0.47 0.29	0.41 0.30	1.0 0.3	24.2 5.6	100	This work

[a] Lifting of discharging voltage in light. [b] Dropping of charging voltage in light. [c] Solar to electrochemical energy conversion and storage efficiency. [d] Extra round-trip efficiency.

10. Supplementary References

1. K. Su, W. Wang, S. Du, C. Ji, M. Zhou and D. Yuan, *J. Am. Chem. Soc.*, 2020, **142**, 18060–18072.

2. Materials Studio DMol3 version 7.0, Density Functional Theory Electronic Structure Program, Copyright. a) B. J. Delley, *Chem. Phys.*, 1990, **92**, 508; b) B. J. Delley, *Chem. Phys.*, 2000, **113**, 7756–7764; c) Accelrys Inc. 2013.

3. J. P. Perdew, K. Burke and M. Ernzerhof, *Phys. Rev. Lett.*, 1996, **77**, 3865.

4. S. Grimme, *J. Comput. Chem.*, 2006, **27**, 1787.

5. A. D. Becke, *J. Chem. Phys.*, 1993, **98**, 5648–5652.

6. Gaussian 16, Revision C.01, M. J. Frisch et al., Gaussian, Inc., Wallingford CT, 2019.

7. A. Paolella, C. Faure, G. Bertoni, S. Marras, A. Guerfi, A. Darwiche, P. Hovington, B. Commarieu, Z. Wang, M. Prato, M. Colombo, S. Monaco, W. Zhu, Z. Feng, A. Vijh, C. George, G. P. Demopoulos, M. Armand and K. Zaghib. *Nat. Commun.*, 2017, **8**, 14643.

8. S. Ahmad, C. George, D. Beesley, J. Baumberg and M. Volder, *Nano Lett.*, 2018. **18,** 1856-1862.

9. C. Xu, X. Zhang, L. Duan, X. Zhang, X. Li and Wei Lü, *Nanoscale*, 2020, **12**, 530-537.

10. B. Boruah, B. Wen and M. De Volder, *Nano Lett.*, 2021, **21,** 3527-3532.

11. K. Kato, A. Puthirath, A. Mojibpour, M. Miroshnikov, S. Satapathy, N. Thangavel, K. Mahankali, L. Dong, L. Arava, G. John, P. Bharadwaj, G. Babu and P. Ajayan, *Nano Lett.*, 2021, **21**, 907-913.

12. J. Lv, Y. X. Tan, J. Xie, R. Yang, M. Yu, S. Sun, M. D. Li, D. Yuan and Y. Wang, *Angew. Chem., Int. Ed. Engl.*, 2018, **57**, 12716–12720.

13. C. Andriamiadamanana, I. Sagaidak, G. Bouteau, C. Davoisne, C. Laberty-Robert and F. Sauvage, *Adv. Sustain. Syst.*, 2018, 1700166.

14. B. D. Boruah, A. Mathieson, S. K. Park, X. Zhang, B. Wen, L. Tan, A. Boies, M. D. Volder, *Adv.*

Energy Mater., 2021, 11, 2100115.

15. B. D. Boruah,* B. Wen, M. D. Volder, *ACS Nano*, 2021, 15, 16616–16624.